J Mater Sci (2011) 46:6046–6053
DOI 10.1007/s10853-011-5566-9

Electrodeposition of thin films and nanowires Ni–Fe alloys, study of their magnetic susceptibility

Céline Rousse · Patrick Fricoteaux

Received: 26 January 2011 / Accepted: 16 April 2011 / Published online: 7 May 2011

Abstract Electrodeposition of thin films and nanowires Ni–Fe alloys is presented. For the thin films, we have studied the impact of various electrolytic conditions (magnetic induction, pH, and substrate) on the composition and magnetic susceptibility. Whatever the electrolytic conditions, the evolution of the composition versus the polarization exhibited first a decrease of the Ni content within the deposit followed by an increase. However, at constant polarization, the obtained values were different. Concerning the evolution of the magnetic susceptibility versus the composition, it is known that it decreases with the enhancement of the Ni percentage. The reason is that the susceptibility of iron is higher than that of Ni. It can also observe a sharp rupture in the evolution of magnetic susceptibility, which appeared near the Invar composition ($Ni_{36}Fe_{64}$). Our results show that the electrolytic conditions do not affect the position of the rupture point for the thin films but modify the susceptibility values. For the nanowires, a polycarbonate membrane has been used as a template. The structural characteristics of wires were examined using X-ray diffraction. According to the composition and as described in the literature for the electrodeposited thin films, a change between the body-centered cubic structure and face-centered cubic structure was obtained for the nanowires. However, for the nanowires this modification appeared for a lower Ni content than for this in thin films. Finally, a comparison of their magnetic susceptibility with thin films exhibited a shift toward the lower Ni contents for the rupture point.

C. Rousse (✉) · P. Fricoteaux
LACM-DTI LRC-CEA 0534/EA4302, UFR Sciences Exactes et Naturelles, B.P.1039, 51687 Reims Cedex 02, France
e-mail: celine.rousse@univ-reims.fr

Introduction

Ni–Fe alloys have been intensively investigated during the last decade for their unique physical properties. Because of its similarity to the Invar ($Ni_{36}Fe_{64}$), this system has generated many attentions due to his anomalous thermal expansion. Report that for this atomic composition, a change of the crystal structure (from bcc for the Fe-rich alloys to fcc for the systems with higher Ni concentration) appears [1–5]. Point out that the magnetic susceptibility of these alloys decreases with the increase of Ni content. It is caused by higher susceptibility of iron than nickel. However, a sharp rupture in the evolution of magnetic susceptibility has been observed near the Invar composition [3, 5]. These results show a large difference according to the elaboration method. Crangle and Hallam [3] have obtained 30% atomic Ni for casting alloys and Ueda and Takahashi [5] have obtained 45% atomic for electrodeposited ones.

The alloy preparation by physical or metallurgical methods presents the advantage of a fine composition control but with a high production cost. Therefore, due to the low fabrication costs, great purity of the deposits, and large choice of the piece shapes, the electrodeposition technique was often favored to prepare many systems. According to Brenner [6], the electrodeposition of Ni–Fe alloys is classified as anomalous, because the less-noble metal (iron) is deposited preferentially. So, many investigations have been achieved in this way [7–12].

Because properties of Ni–Fe electrodeposited alloys are affected by number of factors, and investigations have been carrying out on the electrodeposition conditions as follows: electrolyte composition, pH, polarization, convection, magnetic field superimposition, additional agent,

etc [13–21]. Some authors have studied the influences on the morphology and have noted that the grains size of the materials was strongly depending on the iron amount inside the Ni–Fe codeposit [14, 22–24]. A correlation with hardness and internal stress in the deposits has been also studied [24, 25]. Lewis et al. [26] were interested in the role of the substrate in the development of the Ni–Fe alloys deposits structure. More recently, the fabrication of magnetic nanowires arrays has become a subject of study for both their fundamental science and potential applications (high-density magnetic recording [27], nanoelectrodes, or sensors [28, 29]). Many types of magnetic nanowire arrays have been investigated (metal, alloys, or multi-layer structure) [30], with different techniques such as nanolithography [31], vapor–liquid–solid growth, and electrodeposition [32]. Similar to the thin films, the electrodeposition is an easy and simple technique to elaborate nanowires with a large scale of diameter and length. In this method, thin wires are electrodeposited into nanometer-wide cylindric pores of a porous material. Molecular sieves [33], track-etched polymer membranes [32, 34], and porous anodic alumites [35] are some representative templates.

For Ni–Fe nanowires, most of the investigations had concerned the magnetic properties study versus electrodeposition parameters or template parameters such as pore diameter, length, or templates nature. Aravamudhan et al. [36] have shown that the application of magnetic field during deposition strongly influences on the crystallographic and magnetic properties of the Ni–Fe nanowires.

In this article, we report the elaboration of thin films and nanowires under different conditions. A study of their composition, structure, and magnetic susceptibility versus electrodeposited parameters is presented.

Experimental methods

The electrolyte baths have been prepared with deionized water, and used chemical products were high purity reagents. To obtain a good deposit quality and to reach all the research composition range for our Ni–Fe alloys, we had to investigate various plating baths. The metallic salts which were used were a combination of $NiSO_4{\cdot}6H_2O$ and $FeSO_4{\cdot}7H_2O$, with concentrations between 0.015 and 0.2 mol L^{-1}. KCl (0.5 mol L^{-1}) and boric acid (0.4 mol L^{-1}) were used as a supporting electrolyte or to maintain the solution in acid pH. According to the experiments, the pH was adjusted to 3 or 3.8 by sulfuric acid addition. Finally, saccharin and L-ascorbic acid (0.05 mol L^{-1}) were added to reduce deposit stress and to minimize Fe^{2+} oxidation.

The electrodeposition was carried out in a cylindrical cell with circulating thermostated water maintained at 30 °C. The solution was stirred during electrodeposition.

Electrochemical experiments were conducted with a Tacussel potensiostat–galvanostat PGZ 301. Some experiments were performed under uniform magnetic field superimposition. For that, the electrochemical cell was put into the gap of an electromagnet (Drusch EAM 20G), and the horizontal electrode surface was kept parallel to the magnetic field.

The plating system was based on a classical three-electrode device (Fig. 1). The reference electrode was a commercial saturated mercury sulfate electrode (SSE), and the counter electrode was a nickel plate. The working electrode (0.2 cm^2) was either a copper or a tin substrate for the thin films and a polycarbonate membrane (Watmann) with a random distribution of nanometric pores for the nanowires (pore diameter = 200 nm; thickness = 10 μm; and

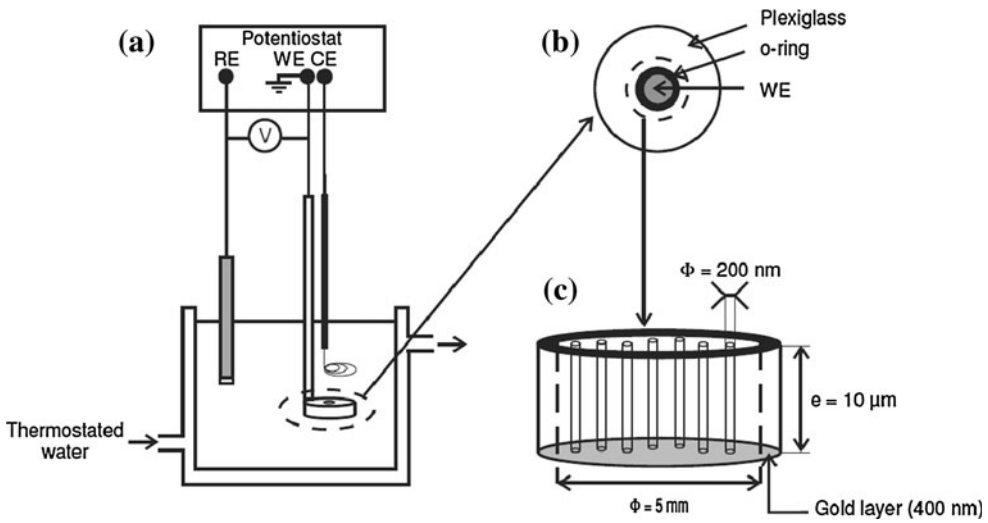

Fig. 1 *a* Schematics of the electrochemical apparatus. *WE* working electrode [polycarbonate membrane (for nanowires electrodeposition) and Cu or Sn substrate (for thin films)]; *RE* reference electrode (SSE); *CE* counter electrode (Pt); *V* voltmeter. *b* Top view of the global working electrode. *c* Detailed view of the polycarbonate membrane

pore density = 3.10^8 pores cm^{-2}). For the last one, metallization of one side of the membrane was necessary to ensure electric contact (400 nm evaporated gold by physical vapor deposition). Before electrolysis, the working electrode was immersed into electrolyte for about 30 min to obtain a good wettability of the membrane pores.

The samples morphology was characterized by a JEOL JSM 6460LA scanning electron microscopy (SEM). Before analysis, the nanowires were released by dissolving the membrane in distilled CH_2Cl_2. The chemical composition was determined by dispersive energy of X-ray spectroscopy (EDXS) or by the ICP-AES technique (Varian-spectrometer). For this last method, the deposit and the substrate were dissolved by oxidation in nitric acid before analysis. Several identical specimens were plated for each operating conditions to ensure a good reproducibility. The crystal structure of nanowires embedded in the polycarbonate was determined by X-ray diffraction with a D8 ADVANCE from BRUCKER using CuKα radiation ($\lambda_{CuK\alpha}$ = 1.54056 Å) to the perpendicular direction of the nanowires. The magnetic susceptibility measurements have been obtained using a home-made Gouy balance with the relationship (1):

$$\chi(\text{a.u.}) = c \cdot (m_B - m_{B=0})/m \quad (1)$$

where χ is the magnetic susceptibility in arbitrary unit, c is a constant, m_B is the read deposit mass in the presence of magnetic field, $m_{B=0}$ is the read deposit mass without magnetic field, and m is the real deposit mass.

Results and discussion

Thin films

Electrochemical study

Whatever the experimental conditions, the current density–potential curves exhibit the same appearance. In all cases, Ni or Fe cannot be plated alone, and the presence of hydrogen co-reduction masks the limiting current diffusion. Some shifts can be seen on the current values versus pH or in the presence of magnetic field (B) (Fig. 2). These differences are due to the competition between the adsorption of Ni^{2+}, Fe^{2+}, and H^+ which could be modified by a presence of convection in the presence of magnetic field or by a different H^+ quantities.

Figure 3 shows nickel content in the deposits versus applied current density (with the same conditions as Fig. 2). Whatever the experimental conditions, the curves present a decrease following by an increase of the Ni content revealing the presence of a competition between the kinetic reduction of nickel, iron, and hydrogen [21]. However, at constant polarization, the obtained Ni atomic

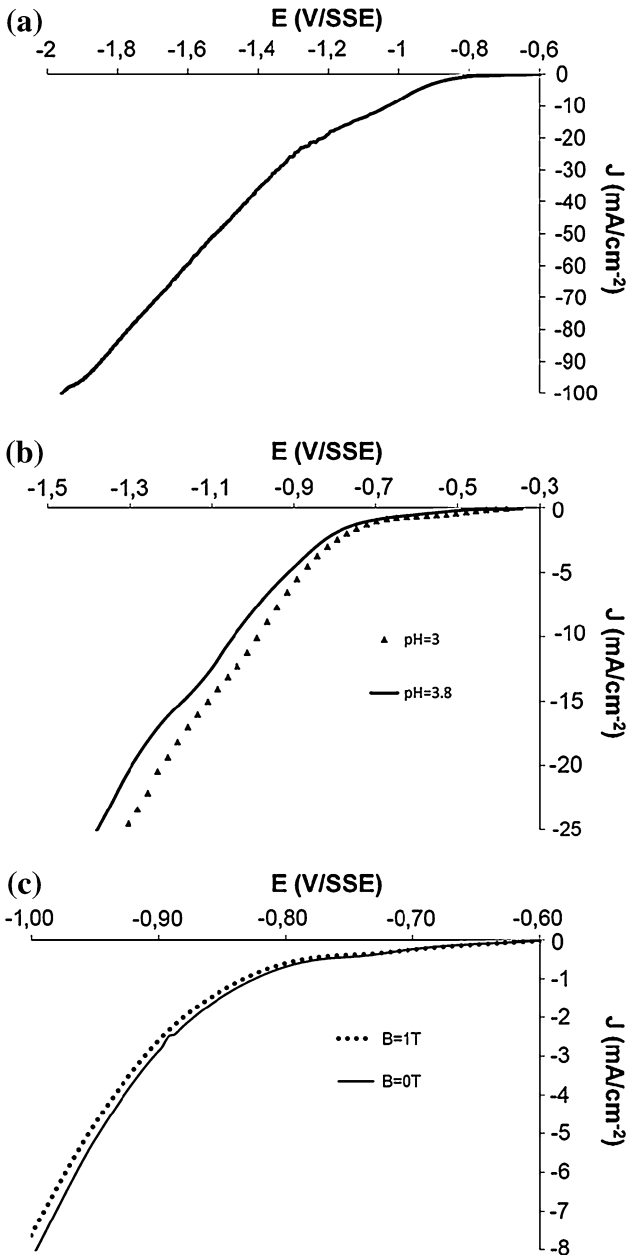

Fig. 2 Current density–potential curve for Ni–Fe systems **a** tin substrate, pH = 3.8, B = 0 T, **b** tin substrate, B = 0 T with either pH = 3 or 3.8, and **c** tin substrate, pH = 3.8, with either B = 0 or 1 T

percentage differs with the pH value (Fig. 2a) or the presence or absence of magnetic induction during the electrolysis (Fig. 2b). These phenomena are principally due to the competition of the Ni^{2+} and Fe^{2+} adsorption according to the electrolytic conditions [6].

Point out that these curves are relatively important to choose the electrodeposition parameters and show that two different current densities may give the same alloy composition.

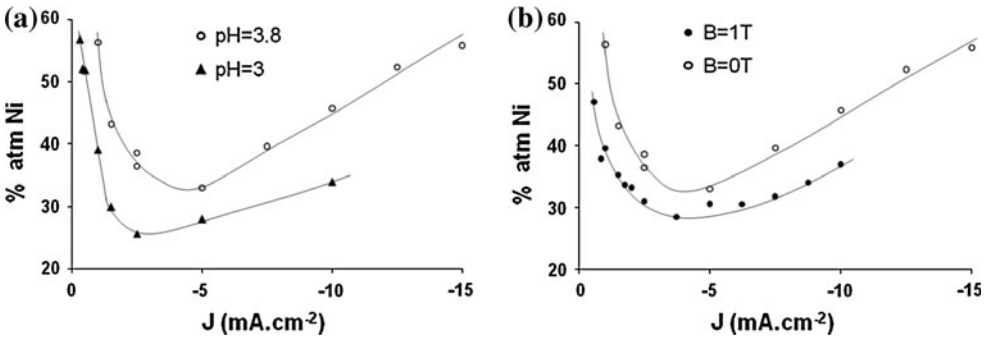

Fig. 3 Nickel atomic content versus current density **a** tin substrate, $B = 0$ T, with either pH = 3 or 3.8 and **b** tin substrate, pH = 3.8, with either $B = 0$ or 1 T

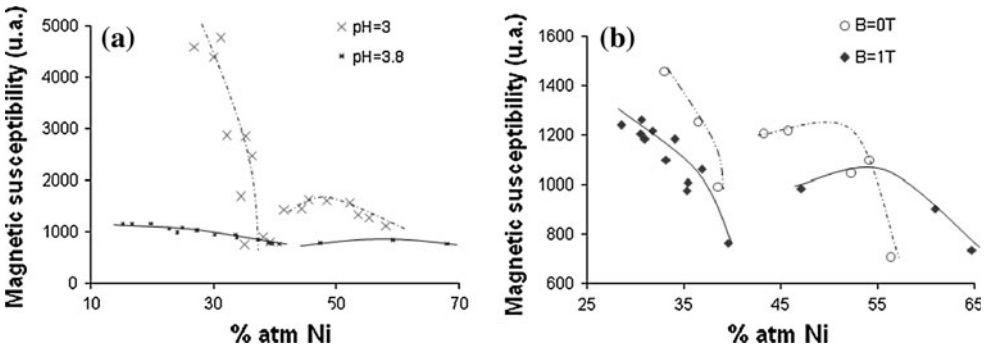

Fig. 4 Magnetic susceptibility (arbitrary unit) versus nickel content **a** copper substrate, $B = 0$ T with either pH = 3 or 3.8 and **b** tin substrate, pH = 3.8 with either $B = 0$ or 1 T

Table 1 Magnetic susceptibility values at the rupture point versus experimental conditions

Substrate	pH	Magnetic induction (T)	% Ni at the top
Thin films			
Sn	3.8	0	40
Cu	3	0	38
Sn	3.8	1	40
Cu	3.8	0	42
Nanowires	3	0	32

Magnetic susceptibility study

A study of the magnetic susceptibility versus nickel content has been made for different electrolytic conditions (pH, magnetic field, and substrate).

Some examples of magnetic susceptibility per mass unit (measured at room temperature) are plotted versus Ni–Fe deposits composition in Fig. 4. For each curve, we observe a rupture of the magnetic susceptibility that is reported in Table 1. The zone for the magnetic susceptibility drop is almost the same whatever our electrodeposition conditions and appears for a nickel content near 40%. Those results are in good concordance with Uedas' values, who obtained the break for 45% atomic Ni with electrodeposited materials [5]. The general aspect of the magnetic susceptibility curves was not modified by electrolytic parameters but the values of magnetic susceptibility depended strongly from them (at constant composition, we obtained different magnetic susceptibility values) and was in good concordance with Ueda's results. The last one finds a body-centered cubic structure (bcc) before the drop magnetic zone and a face-centered cubic structure (fcc) after this one.

Finally, SEM observations were achieved for thin film (Fig. 5). All deposits surfaces obtained near the zone of the magnetization rupture (~35–45% atomic Ni) present a cracked surface with fines grains (Fig. 5a and b). This could be correlated to the internal stresses inside the deposits because of the mixture between bcc and fcc. Samples with composition inferior to 35% atomic Ni and superior to 45% atomic Ni present surface with higher grains sizes. This phenomenon is more accentuated with the higher nickel content (Fig. 5c and d).

Nanowires

Electrochemical study

Figure 6 shows a typical voltammogram for Ni–Fe electrolysis inside a polycarbonate membrane. This curve exhibits that no defined diffusion current can be obtained due to the presence of hydrogen co-reduction. Point out the two particularly points (noted "a" and "b") in this curve. The presence of the point "a" will be explained later. The sudden increase of the cathodic current for the point "b" does not correspond to the hydrogen reduction apparition, but to an increase of the active surface of the working

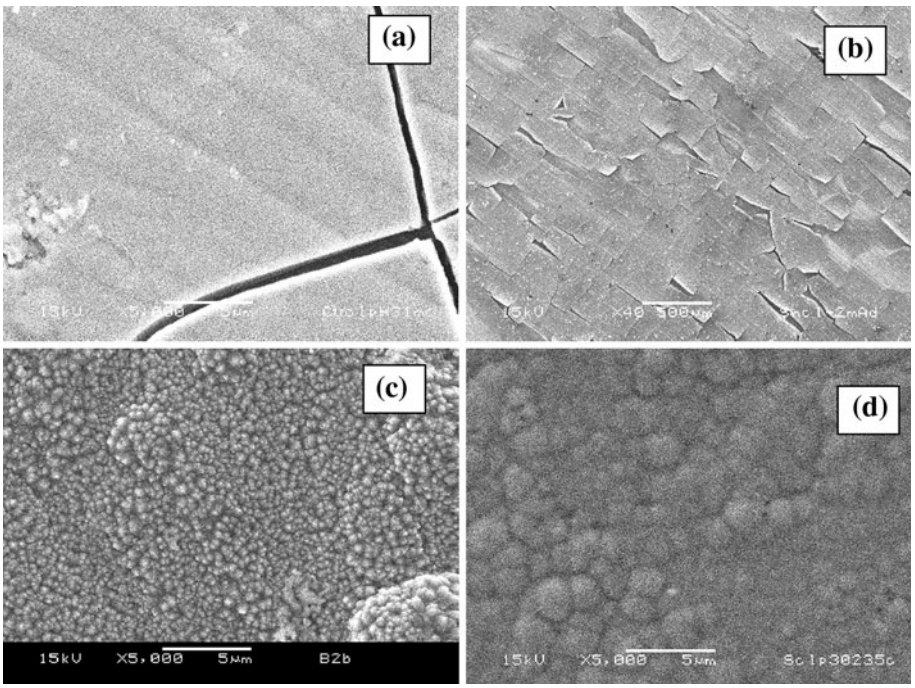

Fig. 5 SEM image of Ni–Fe alloys, **a** and **b** Sn substrate, pH = 3, 35% atomic Ni; **c** Sn substrate, pH = 3, 23% atomic Ni; and **d** Sn substrate, pH = 3, 60% atomic Ni

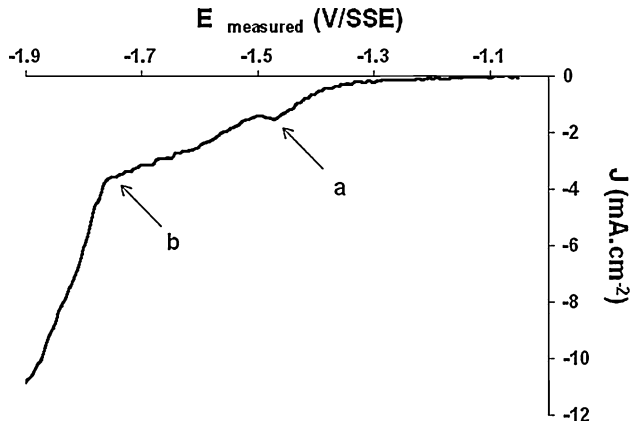

Fig. 6 Current density–potential curve for Ni (0.1 mol L^{-1}) and Fe (0.1 mol L^{-1}) system. Conditions: pH = 3, scanning rate = 2 mV s^{-1}

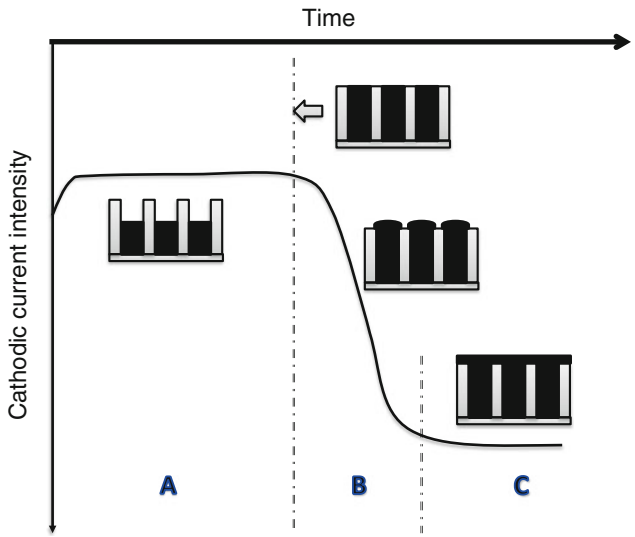

Fig. 7 Schematic current intensity–time curve during template process. The *black* part corresponds to the deposit evolution

electrode when the deposit overflows the membrane. The potential of this point is connected to the speed of scanning. If the scanning is faster, potential is becoming more negative. This is due to a smaller membrane filling in time unit.

On the Fig. 7, we are showing the evolution of the Ni–Fe current reduction at a fixed potential when electrolyze was carried out inside a membrane. Three parts could be noted. In the first one noted A, the current intensity is relatively constant. This part corresponds to the 1D pore-filling procedure. Point out that during the very first seconds of the part A, the current intensity evolves rapidly due to the diffusion phenomenon. The zone B corresponds to the evolution of the active surface of the deposit when this one overflows the membrane (corresponding to the 3D growth). The cathodic current increases as soon as the pores of the membrane are filled. Finally, when entire deposit covered the membrane, the current stabilizes again (zone C).

Figure 8 presents the top view of membrane versus time for an applied potential equal to −1500 mV/SSE. In the zone A, we observe holes, corresponding to the pore of the membrane which is no filled. Point out the presence of a

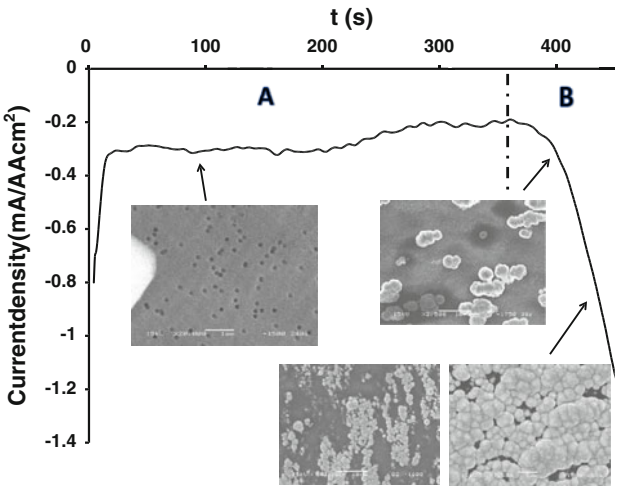

Fig. 8 Current density versus time coupled with SEM picture of membranes (*top view*) Ni (0.1 mol L^{-1}), Fe (0.1 mol L^{-1}), pH = 3, $E = -1500$ V/SSE

discontinuity at approximately 200 s (zone A) attributed to a rapid change in both size and shape of the diffusion layers [37]. At the beginning of the zone B, we detected some nodules corresponding to the overflows of the membrane's pore. At the end of this zone, the surface is totally covered. In our opinion that these changes in the diffusion layer are at the origin of the particular point noted "a" on the Fig. 6.

In Fig. 9, we exhibit SEM pictures for cross-section membranes associated with their EDX profiles. This technique allows us to observe the nanowires inside the templates. In the Fig. 9a, the pores do not reach the top of the membrane. This specimen corresponds to the region A from Figs. 7 and 8. The zone noted number 1 shows the difference between the end of nanowires and the top of the membrane. The EDX analyze (Fig. 9) indicates the presence of Au, Ni, Fe, and C. The presence of gold comes from the gold film deposited for the membrane metallization. Nickel and iron come from the deposit and carbon is due to the polycarbonate membrane. As no deposit is present in the zone 1, only carbon can be detected by EDX. In the Fig. 9b, pores are totally filled. We can note that Ni and Fe overflow the membrane's pores. That is characterized by the zone noted number 2 (region B from Figs. 7 and 8).

Structure study

After dissolution the membrane in CH_2Cl_2, the nanowires were aggregated together in a bunch (Fig. 10). The nanowires are relatively straight and long resulting in a large surface-to-volume ratio. Their diameters are in range between 300 and 350 nm corresponding to a larger more than 60% of the nominal diameter. This fact could be explained by an expansion of the pores during electrodeposition. We noted that nanowires do not have a perfect uniform diameter along the entire axis. This fact was always reported by Motoyama et al. [38], who have made the same observations for Cu and Ni nanowires. Moreover, some little excrescences perpendicular to the nanowire axis (Fig. 10b) could be observed. All of these observations are due to the presence of the defect inside the polycarbonate membranes.

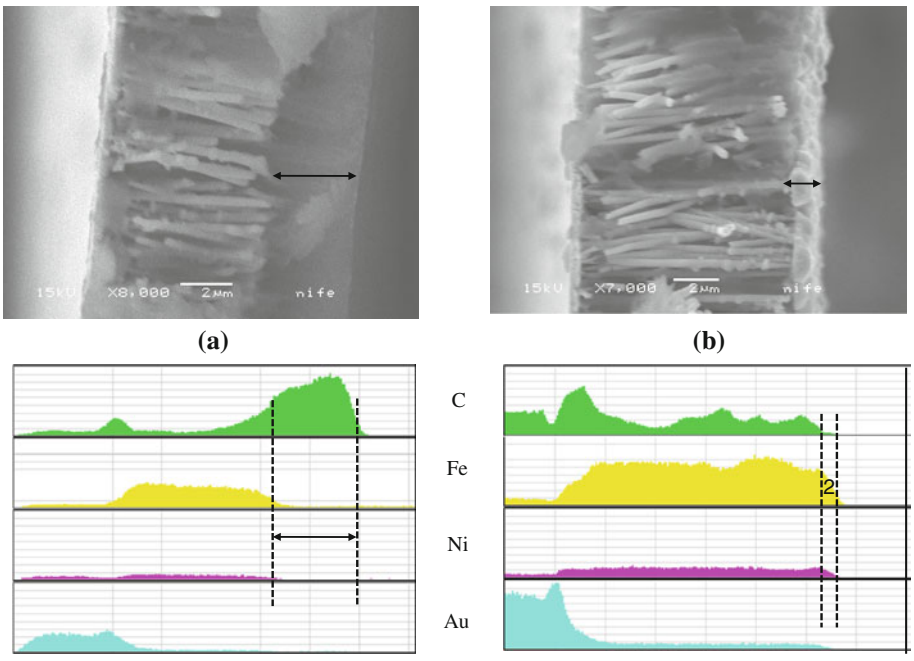

Fig. 9 SEM microphotography for membrane cross section with their associated EDX profile. **a** Zone A from Figs. 7 and 8 and **b** Zone B from Figs. 7 and 8. Bath: Ni (0.1 mol L^{-1}), Fe (0.1 mol L^{-1}), pH = 3, $E = -1500$ V/SSE

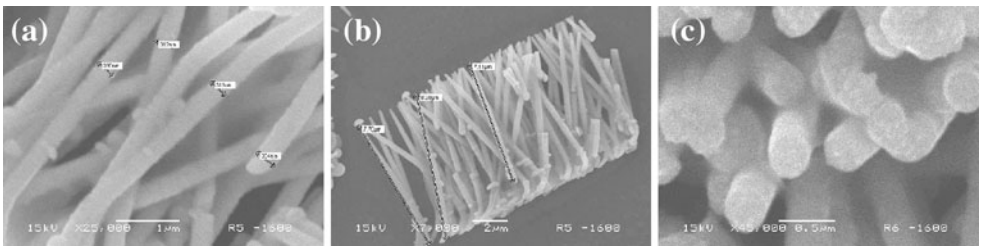

Fig. 10 SEM microphotography of the Ni–Fe nanowires arrays after membrane dissolution Bath: Ni (0.2 mol L^{-1}), Fe (0.06 mol L^{-1}), pH = 3, $E = -1500$ V/SSE

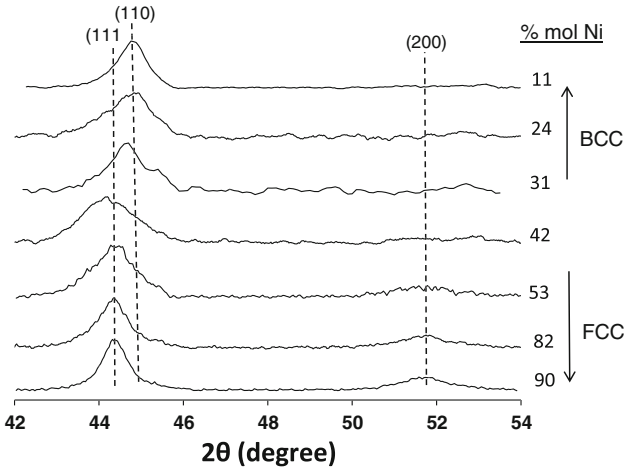

Fig. 11 XRD diffraction patterns of the Ni–Fe nanowires embedded in the membranes

The Fig. 11 represents the evolution of crystalline structure for different compositions of electrodeposited Ni–Fe nanowires embedded in the polycarbonate membrane. All analyzed samples were electrodeposited until the end of the zone A (Figs. 7 and 8). For low nickel content, the nanowires exhibit a bcc structure with a (110) texture. When the Ni content becomes larger (>24%), a mixture between bcc and fcc structure appears. Then, for higher Ni content (>42%), the alloy exhibits a fcc structure with a (111) growth orientation and a significant (200) reflexion. Grimmett et al. [39] have already reported for thin films that the crystalline phases (fcc, bcc, and mixed fcc + bcc) in the electrodeposited alloys depend from alloy composition. Leith et al. [40] have found a phase transition zone between 40 and 50% atomic Ni. For the thin Ni–Fe alloys films, Ueda and Takahashi [5] have shown that the evolution of the region, which formed α phase (bcc) in the film was different from that of the bulk. In our case, for the nanowires, the transition zone seems to move toward less nickel contents.

Magnetic susceptibility study

Similar to the thin films, we have also studied the magnetic susceptibility of our nanowires versus nickel content. The Fig. 12 exhibits the comparison between nanowires and thin films obtained in the same conditions. The same behavior is always observed, but this time, the rupture of the magnetic susceptibility appears for lower nickel content. Point out that this shift is in good accordance with this for the structure change for nanowires.

Fig. 12 Magnetic susceptibility (arbitrary unit) versus nickel atomic content in pH = 3, thin film and nanowires

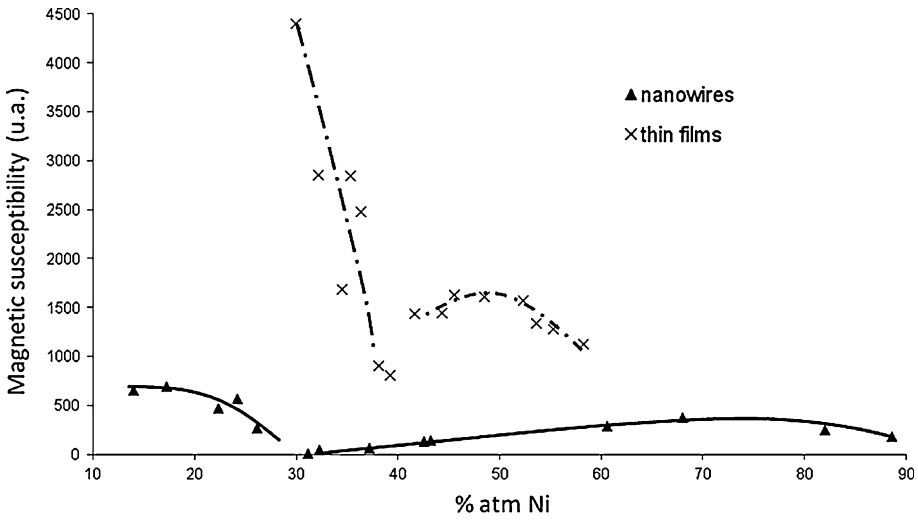

Conclusion

These investigations based on the electrodeposition process of Ni–Fe alloys under different conditions have confirmed changes in the structure and the rupture of the magnetic evolution versus the nickel content for a composition close to Invar alloy.

The pH modification, substrate change, and presence of the magnetic induction during the electrolysis do not affect the rupture point for the magnetic susceptibility. Only modifications of their individual values were observed.

Concerning the nanowires, we have pointed out that their behaviors are the same as for the thin films. However, the structure change and rupture point of the magnetic susceptibility appear for lower nickel content.

Finally, for the extension of this study, the next challenge will be now to analyze the anomalous thermal expansion of the nanowires in this special zone of change.

References

1. Wiess RJ (1963) Proc Phys Soc 82:281
2. Kondorsky EI, Sedov VL (1960) J Appl Phys 31:331S
3. Crangle J, Hallam GG (1963) Proc R Soc Lond 272:119
4. Kouvel JS, Wilson RH (1961) J Appl Phys 32:435
5. Ueda Y, Takahashi M (1980) J Phys Soc Jpn 49:477
6. Brenner A (1963) Electrodeposition of alloys, vol 2. Academic Press Inc, New York
7. Matlosz M (1993) J Electrochem Soc 140:2272
8. Zech N, Podlaha EJ, Landolt D (1999) J Electrochem Soc 146:2886
9. Krause T, Arulnayagam L, Pritzker M (1997) J Electrochem Soc 144:960
10. Afshar A, Dolati AG, Ghorbani M (2003) Mater Chem Phys 77: 352
11. Vaes J, Fransaer J, Celis JP (2000) J Electrochem Soc 147:3718
12. Lachenwitzer A, Magnussen OM (2000) J Phys Chem B 104: 7424
13. Andricacos PC, Arana C, Tabib J, Dukovic J, Romankiw LT (1989) J Electrochem Soc 136:1336
14. Karthik R, Raja RJ, Ramasamy M, Sheela G, Madhu S, Kennedy S, Ramakishan Rao CH, Pushpavanam M (2003) Trans Inst Met Finish 81:68
15. Grimmett DL, Schwartz M, Nobe K (1998) Plat Surf Finish 75:94
16. Ramachandran A, Tharamani CN, Mayanna SM (2001) Trans Inst Met Finish 79:195
17. Ebrahimi F, Ahmed Z (2003) J Appl Electrochem 33:733
18. Msellak K, Chopart JP, Jbara O, Aaboubi O, Amblard J (2004) J Magn Magn Mater 281:295
19. Tabakovic I, Riemer S, Vas'Ko V, Sapozhnikov V, Kief M (2003) J Electrochem Soc 150:C635
20. Rousse C, Msellak K, Fricoteaux P, Merienne E, Chopart JP (2006) Magnetohydrodynamics 42:371
21. Fricoteaux P, Rousse C (2008) J Electroanal Chem 612:9
22. Cheung C, Djuanda F, Erb U, Palumbo G (1995) Nanostruct Mater 5:513
23. Ebrahimi F, Li H (2003) Rev Adv Mater Sci 5:134
24. Li H, Ebrahimi F (2003) Mat Sci Eng A347:93
25. Li H, Ebrahimi F, Choo H, Liaw Peter K (2006) J Mater Sci 41:7636. doi:10.1007/s10853-006-0856-3
26. Lewis DB, Lehmberg CE, Marshall GW (2001) Trans IMF 79:175
27. Sellmyer DJ, Zheng M, Skomski R (2001) J Phys Condens Matter 13:R443
28. MCGary PD, Tan L, Zou J, Stadler BJH, Downey PR, Flatau AB (2006) J Appl Phys 99:08B310
29. Yun M, Myuna NV, Vasquez RP, Wang J, Monbouquette H (2003) Nanofabr Technol Proc SPIE 5220:37
30. Blondel A, Meier JP, Doudin B, Ansermet JPh (1994) Appl Phys Lett 65:3019
31. Chou S, Wei M, Krauss PR, Fischer PB (1994) J Vac Sci Technol B12:3695
32. Fert A, Piraux L (1999) J Magn Magn Mater 200:338
33. Ozin GA (1992) Adv Mater 4:612
34. Martin CR (1994) Science 266:1961
35. Sugawara A, Streblechenko D, McCartney M, Scheinfein MR (1998) IEEE Trans Magn 34:1081
36. Aravamudhan S, Singleton J, Goddard PA, Bhansali S (2009) J Phys D Appl Phys 42:115008
37. Roy E, Fricoteaux P, Yu-Zang K (2001) J Nanosci Nanotechnol 1:1
38. Motoyama M, Fukunaka Y, Sakka T, Ogata YH, Kikuchi S (2005) J Electroanal Chem 584:84
39. Grimmett DL, Schwartz M, Nobe K (1990) J Electrochem Soc 11:3414
40. Leith SD, Ramli S, Schwartz DT (1999) J Electrochem Soc 146:1431